Chemically-tunable formation of different discrete, oligomeric and polymeric self-assembly structures from a di-gold metallo-tweezer

Susana Ibáñez,[a] and Eduardo Peris*[a]

Abstract: We describe a new di-gold metallo-tweezer whose complex supramolecular landscape is controlled by adding a series of metal cations. This metallo-tweezer has a strong tendency to form interesting supramolecular structures upon addition of Tl[+], Ag^{+} and Cu^{+}. The choice of the cation is used to directing the formation of the designated molecular architecture. The addition of thallium facilitates the formation of a self-aggregated duplex structure, with the cation occupying the cavity of the dimer. The same type of structure is formed when Cu^{+} is added, and the resulting duplex inclusion complex displays interesting vapochromism properties. This copper-encapsulated system evolves in solution to a 1-D helical supramolecular polymer displaying multiple aurophilic and Au-Cu interactions, with the copper cation bound to several alkynyl ligands of the tweezer. The addition of a small amount of silver cation to the di-gold tweezer yields a similar type of inclusion dimer complex, but adding an excess of the cation produces new discrete molecules presumably displaying multiple Au-Au, Au-Ag and Ag-Ag metallophilic interactions. The differences in the supramolecular structures formed are ascribed to the different tendency of the metal cations to exhibit interactions with the gold atoms and to coordinate to the alkynyl ligands of the tweezer.

Introduction

For the design of materials with tailor-made applications, it is necessary to develop synthetic procedures that lead to structures with programmed and controllable architectures. In this regard, the research in self-assembling supramolecular systems is a field of increasing interest, because it sets the basis for providing rational ways for the generation of functional materials.[1] The driving forces that enable self-aggregated materials stems from the ability of the smaller molecular entities to arrange spontaneously into more organized systems, but the monitoring of the assembly process and the comprehensive control of the final structures are often elusive.[2] From the synthetic point of view, the use of metalloligands brings unique opportunities, because the utilization of well-defined coordination compounds as building blocks offers structural rigidity by placing the auxiliary functional groups at pre-organized conformations.[3]

[a] Dr. S. Ibáñez, and Prof. E. Peris
    Institute of Advanced Materials (INAM). Universitat Jaume I. Av. Vicente Sos Baynat s/n. Castellón. E-1271. Spain. Email: eperis@uji.es

    Supporting information for this article is given via a link at the end of the document.

Metalloligands -defined as metal complexes capable of binding other transition metals- also allow the facile synthesis of heterometallic supramolecular structures, which are otherwise difficult to achieve. Most metalloligands consist of metallorganic units bearing Werner-type ancillary binding groups (N-, O-, P-, donor atoms), or hydrogen-bond donors, which facilitate the self-assembly of the desired molecule. Among the non-covalent intermolecular interactions, attractive metallophilic interactions,[4] especially those observed for Au(I), have been increasingly utilized as a design element to synthesize functional high-dimension systems.[5] The existence of metallophilic interactions in supramolecular assemblies has given rise to a large number of materials exhibiting photoluminescence and vapochromic properties, of great relevance for the applications in luminescence signaling and vapochemical sensing.[6] Gold alkynyls[7] are recently being regarded as an extremely interesting type of organometallic-based metalloligands due to their potential binding abilities via the alkynyl ligand and through aurophilic/metallophilic interactions.[8] In this context, we recently became interested in the preparation of di-gold(I) metallo-tweezers containing bis-alkynyl linkers for the recognition of metal cations[9] and polycyclic aromatic hydrocarbons (PAHs).[10] In the first of the examples, a gold(I) metallo-tweezer with a bis-alkynyl linker and terminal pyrene-functionalized N-heterocyclic carbenes (**1** in Scheme 1), was able to dimerize in the presence of 'naked' M[+] ions (M = Cu, Tl and Ag) as a consequence of π-stacking and metallophilic interactions. Such dimerization produced the encapsulation of the metal cation inside the cavity of the dimer, giving rise to discrete self-aggregated duplex structures showing metallophilic interactions between M[+] and the surrounding four Au atoms of the structure (**2**). Some other authors have provided very interesting examples of the use of non-covalent complexation between tweezers and metal-containing guests as a strategy for endowing short-range metal-metal interactions.[6i, 11]
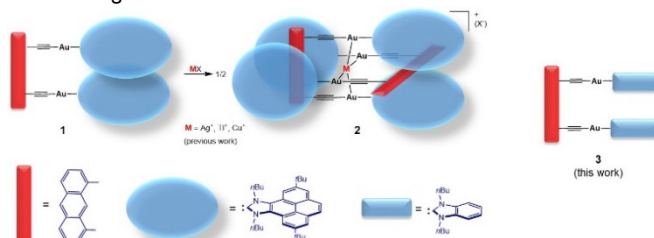
Scheme 1. Gold-based metallo-tweezers.

Results and Discussion

Complex **3** was obtained by reaction of 1,8-diethynylanthracene with [Au(NHC)Cl] (NHC = N,N'-di-*n*butyl-benzimidazolylidene) in methanol in the presence of NaOH. The complex was characterized by NMR spectroscopy and elemental analysis. Both the ^{1}H and ^{13}C NMR spectra were consistent with the pseudo-C_{2v} geometry of the molecule. The ^{13}C NMR spectrum revealed the resonance due to the two equivalent metallated Au-$C_{carbene}$ carbons at 194.9 ppm. By performing a series of ^{1}H NMR spectra of **3** in CDCl$_3$ at different concentrations (0.33-21mM) we observed that the proton resonances did not show any changes, therefore we concluded negligible self-aggregation of the complex in this solvent (see Figure S12 in the Supplementary Information). The molecular structure of **3** was determined by X-ray crystallography. The structure of **3** (Figure 1) consists of two Au(I)-benzimidazolylidene units connected by the anthracenyl-bis-alkynyl ligand. The two arms of the tweezer that are connected by the anthracenyl linker progressively approach to each other, as reflected by the distances between the α-atoms of the alkynyl ligand (C3-C4, 4.95 Å), the two gold centers (Au1-Au2, 4.35 Å), and the planes defined by the benzene fragments of the benzimidazolylidene ligands (3.44 Å). This suggests that the shape of the tweezer is highly influenced by the intramolecular π-staking of the terminal benzimidazolylidenes. The structure of **3** differs from the solid state structure of **1**, which showed the formation of a self-aggregated duplex complex by the self-association of two molecules of the tweezer.[9] The fact that **3** does not form such type of a self-aggregated complex indicates that the substitution of the pyrene-imidazolylidene ligand (in **1**) by a benzimidazolylidene (in **3**) reduces the ability of the molecule to self-aggregate in the absence of external stimuli.
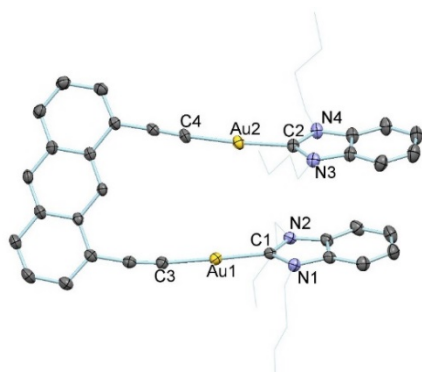
previously observed for complex **1**.[9] All three complexes (**4**, **5** and **6**, according to Scheme 2) were isolated in yields ranging from 75-90 %, and were characterized by NMR spectroscopy and mass spectrometry, and gave satisfactory elemental analyses. The ^{1}H NMR spectra of all three products showed that the signals due to the protons of the anthracene linker and of the aromatic protons of the imidazolylidene, are significantly upfield shifted with respect to the related signals in **3**, therefore suggesting significant π–π-stacking contacts. The analysis of the complexes by time-of-flight-mass-spectrometry (TOFMS), revealed main peaks at m/z 2361.7, 2265.5 and 2220.6, which corresponded to the mass of two molecules of **3** plus the mass of Tl$^+$, Ag$^+$ and Cu$^+$, for the spectra of **4**, **5** and **6**, respectively, in clear agreement with the proposed structures.
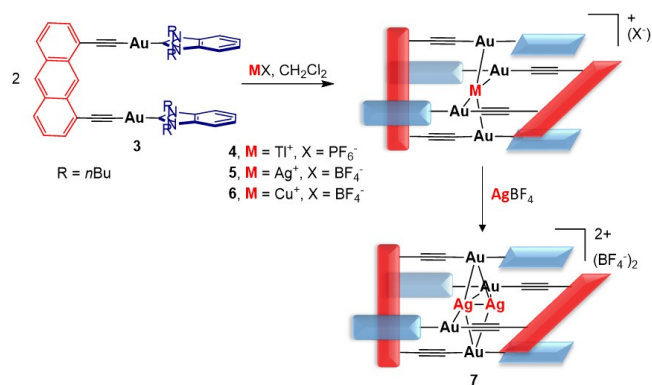
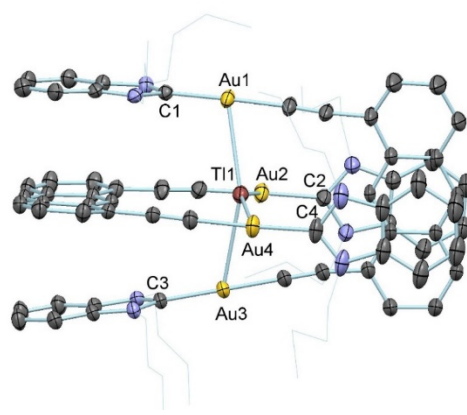**Scheme 2.** Metal-triggered self-association

Figure 1. Molecular structure of **3**. Hydrogen atoms and solvent (CH2Cl2) were removed for clarity. nBu groups are represented in the wireframe style for clarity. Ellipsoids at 50% probability. Selected distances (Å) and angles(º): Au(1)-C(1) 2.010(4), Au(1)-C(3) 1.982(4), Au(2)-C(2) 2.017(4), Au(2)-C(4) 1.985(4), C(3)-Au(1)-C(1) 178.65(15), C(4)-Au(2)-C(2) 175.95(16).

Figure 2. Molecular structure of **4**. Hydrogen atoms, solvent (CHCl$_3$) and counter ion (PF$_6$⁻) were removed for clarity. *n*Bu groups are represented in the wireframe style for clarity. Ellipsoids at 50% probability. Selected distances (Å): Au(1)-C(1) 2.004(9), Au(2)-C(2) 2.008(10), Au(3)-C(3) 2.035(9), Au(4)-C(4) 2.014(11), Au(1)-Tl(1) 3.0503(7), Au(2)-Tl(1) 3.0898(7), Au(3)-Tl(1) 3.1163(6), Au(4)-Tl(1) 3.0630(7).

We wanted to test if complex **3** would be a good receptor for the recognition of Tl$^+$, Ag$^+$ and Cu$^+$ and compare its abilities to those shown by **1**. The reaction of **3** with 0.5 equivalents of MX in CH$_2$Cl$_2$ (MX = TlPF$_6$, AgBF$_4$ and [Cu(CH$_3$CN)$_4$]BF$_4$) promoted the self-aggregation of the di-gold complex and the trapping of the metal cations in the cavity formed, in a very similar manner to that

The molecular structure of **4** was confirmed by single crystal X-ray diffraction (Figure 2). The structure shows that a Tl$^+$ ion is encapsulated inside of a **3**$_2$ dimer. A PF$_6$⁻ anion balances the positive charge of the resulting structure. The thallium cation is surrounded by four gold atoms, with which it establishes close Au···Tl contacts, with distances ranging from 3.05 to 3.11 Å.

The formation of complexes **4**, **5** and **6** was monitored by ^{1}H NMR spectroscopy in CDCl$_3$. In all cases (see SI for details), the addition of sub-stoichiometric amounts of metal cations (<0.5 equivalents) resulted in the appearance of two species, assigned to unreacted **3** and to the self-aggregated species formed by reaction with the metal cations (**4**, **5** or **6**). This result indicates that the exchange between **3** and free M[+], and the self-assembly complexes (**4-6**) is slow on the NMR timescale. In the case of the addition of TlPF$_6$ and [Cu(CH$_3$CN)$_4$]BF$_4$ the addition of excess of the cation (> 1 equivalent) did not produce any changes on resulting ^{1}H NMR spectra, indicating that **4** and **6** are stable species which do not evolve in the presence of an excess of either of these to cations. The situation is different for the titrations with Ag^{+}. For this case, the addition of an excess of the cation showed the evolution of the reaction to a new complex species (**7**, in Scheme 2). This species was characterized by NMR spectroscopy and gave satisfactory elemental analysis. The TOF-mass spectrum of **7** reveals two main peaks at m/z 2265.5 and 1186.3, assigned to [**7**-BF$_4$][+] and [**7**-2(BF$_4$)][2+], respectively. This species can be regarded as the inclusion complex (Ag^{+})$_2$@**3**$_2$, whose structure is supported by the ^{1}H NMR spectrum, which evidences the shielding of the signals of the protons of the anthracene and the benzimidazolylidene compared to the related ones in **3**, therefore strongly suggesting self-aggregation by π–π-stacking. The formation of **7** and thus, the different behavior of Ag^{+} compared to Tl[+] and Cu^{+} in these experiments, may be explained as a consequence of the maximization of the Au···Ag contacts, and the σ-bonds established by the η^2-alkynyl and the silver atoms. The complex would very likely be additionally stabilized by the presence of Ag···Ag argentophilic interactions. The lower ability of Tl to bind to alkynes, and the lower tendency of Cu to undergo Cu···Cu contacts may justify the different behavior of these two metals. Unfortunately, we were not able to grow crystals suitable for X-ray diffraction of **7**, because the complex slowly evolved to a new species in solution, whose nature was elucidated by X-ray diffraction (*vide infra*).

In order to obtain information about the association process of **3** with the three different metal cations, we performed Uv-Vis and fluorescence titrations. In all cases, the spectrometric titrations showed clear isosbestic (for UV) and isoemissive (fluorescence) points, indicating that the formation of the duplex complexes **4-6** proceeded without the involvement of any detectable intermediate species. The electronic absorption spectrum of **3** in CH$_2$Cl$_2$ at 298 K is dominated by an intense broad band at 250-300 nm assigned to the intraligand (IL) π–π* transition of the alkynyls, and the bands at 420, 400, 378, 359 and 342 nm, which are assigned to metal-perturbed IL transitions of the anthracenyl linker. Upon addition of the metal cations, the intensity of these latter bands decreases, while a new set of lower energy bands appear ($\Delta\lambda_{av}$ = +20 nm). In addition, a new broad band centered at 324 nm appears. The growth of this new band is associated with the M-π (alkynyl) core (the π* C≡C orbital decreases in energy upon coordination to M).[12] The emission spectrum of **3** shows a vibronically resolved band centered at 430 nm, which is coincident with the typical monomer band of anthracene as shown in related anthracene-diacetylide di-gold(I) complexes.[13] The addition of incremental amounts of M[+] gradually produced the appearance of two broad

bands centered at 376 and 394 nm. Similar to the electronic absorption titrations, the appearance of these new bands is attributed to the formation of non-covalent M-Au interactions upon encapsulation of the metal cations. In addition, the emission bands due to the anthracenyl linker are shifted by ≈15 nm, which we attribute to a change of the metal-perturbed ligand centered transition, as a consequence of the Au···M contacts. All details are given in the electronic supplementary information.
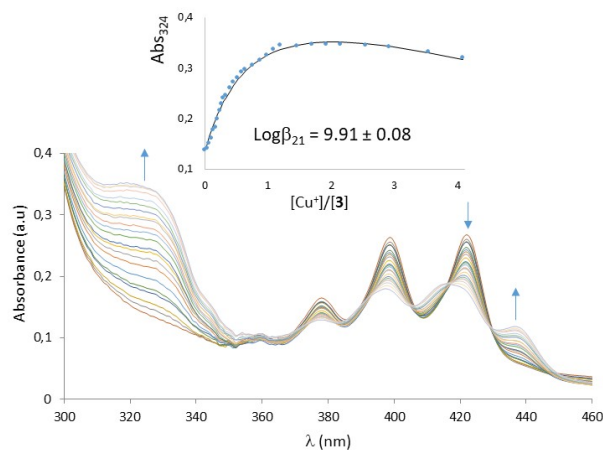

Figure 3. Uv-vis spectra acquired during the titration of **3** (1x10^{-5} M) with [Cu(NCMe)$_4$]BF$_4$ in CH$_2$Cl$_2$ at 298K. The plot represents Abs$_{324}$ (absorbance at 324 nm) against the [Cu^{+}]/[**3**] ratio. Blue dots are the experimental values, and solid black line represent the theoretical fit assuming a 2:1 binding model.

The analysis of the binding isotherms generated from both types of measurements clearly revealed that the titrations should provide rather reliable results, since the final part of the titrations clearly trended to reach a plateau, therefore indicating quasi-quantitative formation of the products. Figure 3 shows the changes observed in the Uv-vis titration of **3** with [Cu(NCMe)$_4$](BF$_4$).

The nonlinear least-square analysis of the Uv-vis and fluorescence titrations to form complexes **4-6** allowed calculating the related association constants with low residual errors when a 2:1 model was used (1:1 and 2:1 models were also tested, but these were discarded due to the lower quality of the fittings).[14] The fittings returned very low values for the K$_{11}$ constants (those leading to the M[+]@**3** products), indicating that the formation of the M[+]@**3** intermediates was negligible all along the titration course. This is illustrated by the speciation plots derived from by the fit of the titration data, which are shown in the supplementary material. This result is in clear agreement with the presence of neat isoemissive and isosbestic points in the series of emission and Uv-vis spectra resulting from the titrations, which strongly suggest that two main species are in equilibrium all along the titrations, as previously discussed. The global association constants (β_{21}) resulting from our calculations are in the range of 10[10]-10[11] M^{-2}, therefore indicating very high binding affinities. Table 1 shows the

association constants derived from the fitting of the data obtained from Uv-vis and emission titrations, where it can be observed that both types of titrations returned values in very reasonable agreement.

Table 1. Global association constants ($\log\beta_{21}$) determined from the fitting of the binding isotherms resulting from the Uv-vis and emission titrations.

Cation	Complex obtained	$\log\beta_{21}$ (Uv-vis)	$\log\beta_{21}$ (Emission)
Tl^+	**4**	10.6 ± 0.1	11.0 ± 0.3
Ag^+	**5**	10.5 ± 0.1	10.7 ± 0.1
Cu^+	**6**	9.91 ± 0.08	10.30 ± 0.08

[a]$\log\beta_{21}$ values calculated by global nonlinear regression analysis using the data obtained from the Uv-vis and emission titrations. Titrations were carried out using constant concentrations of host (10^{-5} M) in CH_2Cl_2 at 298 K. Errors refer to the regression fittings. All data used for the calculations are given in the Supplementary Information.

We observed that complex **6** displayed very interesting vapochromic behavior. Materials displaying Au-Cu contacts that show switching of color and/or luminescence upon application of an external stimulus remain very scarce,[6d, 15] and there are very few examples describing the vapor-responsive behavior related to alkynyl complexes of coinage metals.[6d, 15d, 16] The vapochromic behavior of d^{10} complexes of the copper subgroup are mostly due to variations in metal-metal distances upon the absorption of volatile organic compounds (VOC). A solid sample of **6** displays naked-eye perceivable color change response to acetonitrile and ammonia vapors. The orange solid turns yellow upon exposure to acetonitrile (or ammonia) vapors during five minutes (Figure 4). Upon exposure to air, the color of the solid reverts to orange just after a few minutes. This color conversion process is fully reversible, as demonstrated through numerous cycles without trace of decomposition.
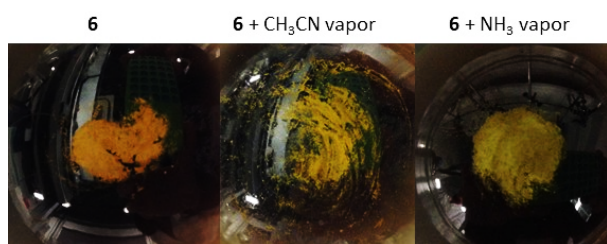

6 **6** + CH_3CN vapor **6** + NH_3 vapor

Figure 4. Photographic images of **6** before (left), and after being exposed to CH_3CN (middle) and NH_3 (right) vapours for 5 minutes.

Gravimetric measurements indicate sorption of up to 4 equivalents of acetonitrile per equivalent of Cu^+, thus strongly suggesting the conversion of **6** into **3**, with the concomitant formation of $[Cu(CH_3CN)_4]^+(BF_4^-)$. In a parallel experiment, we performed the ^1H NMR spectrum of **6** in $CDCl_3$ and observed its transformation into **3** upon addition of CD_3CN to the solution. These experiments clearly support that the conversion between **6** and **3** is driven by the presence of CH_3CN, thus providing a very plausible explanation for the reversible vapochromism shown by

6. Complex **6** was insensitive to the presence of vapors of other organic substrates, such as pyridine, diethyl ether or methanol. On the other hand, the Tl and Ag related complexes **4** and **5** did not show any perceivable vapochromic behavior.
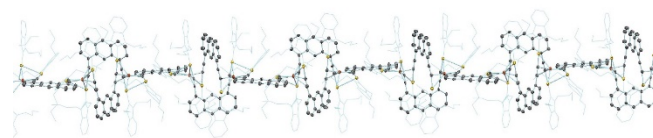

Figure 5. Molecular structure of polymer **8**. Solvent (CH_2Cl_2), counter-anions (BF_4^-) and hydrogens have been removed for clarity. Benzimidazolylidene ligands are represented in the wireframe form. Gold atoms in yellow, copper atoms in orange.
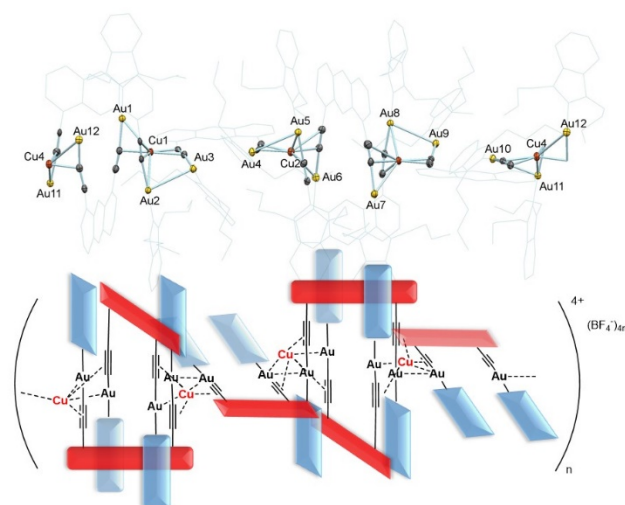

Figure 6. Simplified molecular view of the asymmetric unit of **8**, representing the disposition of the metal atoms in the structure, and displaying the most important bonding interactions. The image below represents a schematic view of the asymmetric unit of the molecule (anthracenyl linkers in red, benzimidazolylidenes in light blue).

Remarkably, crystallization of a long-standing solution (one day, room temperature) of **6** in CH_2Cl_2 gave the polymeric chain **8** (Figure 5), whose structure was determined by X-ray diffraction. The asymmetric unit of this supramolecular polymer consists of six molecules of **3** and four Cu^+ cations, connected by multiple metallophilic Au-Au and Au-Cu interactions, and by the η^2-coordination of the alkynyl fragments to the Cu atoms (Figure 6). The chain is extended along the *c* axis of the cell, displaying a helical conformation. The polymer may be viewed as a series of self-aggregated duplex structures of **3** linked by an orthogonally disposed additional molecule of **3** (see the simplified drawing shown in Figure 6). Each copper atom is coordinated to three alkynyl ligands of adjacent molecules of **3**, and establishes close contacts with two gold atoms, also of adjacent units. The Au-Cu bond distances range between 2.79-2.84 Å. Two out of every three gold centers are showing strong Au-Au interactions, with distances ranging between 3.09 and 3.13 Å.

Polymer **8** is the product of the evolution of **6** in CH_2Cl_2 solution, not only a solid material formed in the crystallization process. In fact, crystals of **8** can be redissolved in $CDCl_3$ and analysed by NMR spectroscopy. The ^{1}H NMR spectrum of the resulting solution is fully consistent with the structure of the polymer, showing two distinctive sets of signals assigned to the two inequivalent types of anthracenyl groups. These observations are a clear evidence that the polymeric nature of the product is preserved in solution.

Confocal fluorescence was used to examine the slow crystallization of **8**. The evaporation of a solution of **8** in CH_2Cl_2 (obtained by dissolving crystals of **8**) rapidly gave micro-rods of about 30 μm long (Figure 7), which showed an emission maximum at 483 nm. The same experiment was carried out using a solution of **8** in CH_2Cl_2/CH_3CN (10:1). In this case, we observed that a solid was formed not showing any particular morphological features, and the emission spectrum of the resulting solid showed a maximum coincident with that of **3**.
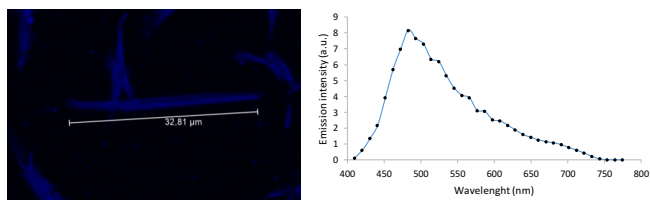

Figure 7. Confocal fluorescence microscopy image of **8**, and emission spectrum recorded.

The formation of polymer **8** needs further explanation, since the stoichiometry of this material differs from that shown by **6**, despite the polymer being a product evolving from this species. The analysis of the mother liquor resulting from the crystallization of **8**, revealed that this solution contained small amounts of $[Au(NHC)_2]^+$ (NHC = N,N'-di-*n*butyl-benzimidazolylidene). This observation indicates that **6** slowly releases Au(I) in the form of $[Au(NHC)_2]^+$, and this should explain why the Cu/Au ratio in **8** (1/3) is higher compared to that shown in **6** (1/4). The evolution of **6** to form **8** needs further rearrangement with loss of the anthracenyl-bis-alkynyl ligand, for obvious stoichiometric reasons, but, unfortunately, we could not determine the fate of this fragment of the molecule.

When attempting to grow crystals of the Ag^{+} inclusion complex **7** from a CH_2Cl_2 solution, we also obtained a product of the evolution of the expected complex (**9**, Figure 8a). In this case, we were also able to obtain crystals suitable for X-ray diffraction of this new species, although the resulting crystal structure is below the standards required for publication. However, the structure contains fully reliable data regarding the nature of the resulting heterometallic di-cationic species formed. We included several ORTEP perspectives of the cation in the Supplementary Information (Figure S6). Figure 8a displays a schematic drawing of **9**. The molecule contains two tri-gold units bound together by multiple Au-Ag interactions, and by interactions of the Ag^{+} cations with the alkynyl ligands. Each tri-gold unit contains two bis-alkynyl-anthracenyl linkers, and two benzoimidazolylidene

ligands at the edges. The two anthracenyl fragments of each tri-gold unit are displaying π–π-stacking contacts with the two antrhracenyl fragments of the complementary tri-Au unit. Each silver atom shows close contacts with two gold and one silver atoms. As in the formation of polymer **8**, the mother liquor left in the crystallization of **9** contained important amounts of $[Au(NHC)_2]^+$, therefore indicating that a CH_2Cl_2 solution of **7** evolves to **9**, as shown in the equation shown in Figure 8b.
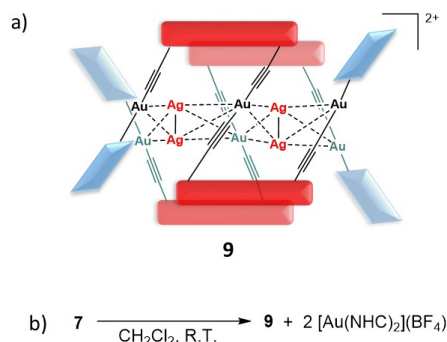

Figure 8. a) Schematic representation of compound **9** (anthracenyl linkers in red, benzimidazolylidenes in light blue). b) Reaction of formation of **9** from **7**.

Conclusions

Our studies show how the molecular tweezer **3** interacts with three different metal cations. The choice of the cation is used to direct the formation of the designated molecular architecture. In principle, the addition of 0.5 equivalents of the metal cation has a similar effect regardless the nature of the cation. In all three cases an inclusion duplex complex is formed, with the cation trapped within the cavity generated inside the self-aggregated structure. Despite their similar structural features, all three species obtained show very distinctive behaviors. While the complexes containing thallium and silver are inert to the presence of acetonitrile or ammonia vapors, the complex with copper shows an interesting reversible eye-perceivable vapochromic behavior in the presence of these two reagents. In addition, solutions of the thallium-trapped species are stable during days, but the compounds containing copper and silver evolve to a 1-D polymer and to an oligomer, respectively. We interpret this different behavior to the tendency of copper and silver to bind to the π-C≡C bond of the alkynyl groups, thus favoring the formation of larger aggregates that involve a larger number of di-gold units, as metallophilic interactions are also maximized. The different behavior between the silver and copper species resides in the higher tendency of silver to form M··M contacts, as reflected in the structure of the Ag-containing oligomer formed.

In conclusion, it is envisaged that the careful control of these directional interactions may constitute an important driving force for the precise tuning of the self-assembly of metallo-supramolecular structures into well-defined structures with interesting functional properties.

Experimental Section

General considerations

1,8-Diethynylanthracene,[17] [Au(NHC)Cl)] (NHC = N,N'-di-*n*butyl-benzimidazolylidene)[18] and [Cu(MeCN)$_4$]BF$_4$[19] were prepared according to literature methods. All other reagents were used as received from commercial suppliers. NMR spectra were recorded on a Bruker 400 MHz or 500 MHz using CDCl$_3$ as solvent. Infrared spectra (FTIR) were performed on a FT/IR-6200 (Jasco) spectrometer equipped with a Pro One ATR (Jasco) with a spectral window of 4000-400 cm^{-1}. Electrospray mass spectra (ESI-MS) were recorded on a Micromass Quatro LC instrument; nitrogen was employed as drying and nebulizing gas. High Resolution Mass Spectra (HRMS) were recorded on a Q-TOF Premier mass spectrometer (Waters) with an electrospray source operating in the V-mode. Nitrogen was used as the drying and cone gas at flow rates of 300 and 30 Lh^{-1}, respectively. The temperature of the source block was set to 120ºC, and the desolvation temperature was set to 150ºC. Capillary voltage of 3.5 kV was used in the positive scan modes and the cone voltage was adjusted typically to 20 V. Mass calibration was performed by using solutions of NaI in isopropanol/water (1:1) from *m/z* 50 to 3000. Elemental analyses were carried out on a TruSpec Micro Series. UV-vis absorption spectra were recorded on a Varian Cary 300 BIO spectrophotometer using CH$_2$Cl$_2$ under ambient conditions. UV-vis absorption spectra were recorded on a Varian Cary 500 spectrophotometer in solid state. Emission spectra were recorded on a modular Horiba FluoroLog-3 spectrofluorometer employing degassed CH$_2$Cl$_2$. Confocal laser scanning microscopy was recorded on a Leica TCS SP8 Inverted Confocal Microscope.

Synthesis of complexes

Synthesis of 3. NaOH (28.56 mg, 0.714 mmol) and 1,8-diethynylanthracene (11.53 mg, 0.051 mmol) were placed together in a round bottom flask and dissolved in methanol (20 mL). This mixture was heated at reflux for 30 min. Then, [Au(NHC)Cl)] (NHC = N,N'-di-*n*butyl-benzimidazolylidene) (50.00 mg, 0.102 mmol) was added as a solid and the resulting suspension was heated at reflux for 4 h. The resulting yellow solid was collected by filtration and washed with methanol and *n*-pentane. Complex **3** (55.40 mg, 93 %) was isolated as a yellow solid. IR (ATR): ν(C≡C): 2101 cm^{-1}. Electrospray MS (20 V, *m/z*): 1079.6 [M+H]$^+$, 1101.6 [M+Na]$^+$. Anal. Calcd. for C$_{48}$H$_{52}$N$_4$Au$_2$·CH$_2$Cl$_2$ (1162.3): C, 50.58; H, 4.68; N, 4.82. Found: C, 50.52; H, 4.63; N, 4.77. ^{1}H NMR (400 MHz, 298 K, CDCl$_3$): δ 10.15 (s, 1H, C*H*$_{anth}$), 8.34 (s, 1H, C*H*$_{anth}$), 7.84 (d, $^3J_{H-H}$ = 8.0 Hz, 2H, C*H*$_{anth}$), 7.70 (d, $^3J_{H-H}$ = 4.0 Hz, 2H, C*H*$_{anth,}$), 7.36 (dd, $^3J_{H-H}$ = 8.0 Hz, $^3J_{H-H}$ = 4 Hz, 2H, C*H*$_{anth}$)), 7.22-7.20 (m, 4H, C*H*$_{Ph}$), 7.03-7.01 (m, 4H, C*H*$_{Ph}$), 4.25 (t, $^3J_{H-H}$ = 8 Hz, 8H, NC*H*$_2$CH$_2$CH$_2$CH$_3$), 1.86-1.70 (m, 8H, NCH$_2$C*H*$_2$CH$_2$CH$_3$), 1.49-1.22 (m, 8H, NCH$_2$CH$_2$C*H*$_2$CH$_3$), 0.88 (t, $^3J_{H-H}$ = 8 Hz, 12H, NCH$_2$CH$_2$CH$_2$C*H*$_3$). ^{13}C NMR (100 MHz, 298 K, CDCl$_3$): δ 194.87 (Au-*C*$_{carbene}$), 136.63 (*C*$_{q\ anth}$), 133.02 (*C*$_{q\ Ph}$), 132.84 (*C*$_{q\ anth}$), 131.71 (*C*$_{q\ anth}$), 129.25 (*C*H_{anth}), 127.21 (*C*H_{anth}), 126.75 (*C*H_{anth}), 126.33 (*C*H_{anth}), 125.09 (*C*H_{anth}), 124.75 (*C*$_{q\ acetylide}$), 123.94 (*C*H_{Ph}), 111.05 (*C*H_{Ph}), 103.65 (*C*$_{q\ acetylide}$), 48.41 (N*C*H$_2$CH$_2$CH$_2$CH$_3$), 32.36 (NCH$_2$*C*H$_2$CH$_2$CH$_3$), 20.24 (NCH$_2$CH$_2$*C*H$_2$CH$_3$), 13.91 (NCH$_2$CH$_2$CH$_2$*C*H$_3$).

Synthesis of 4. A solution of **3** (100.00 mg, 0.093 mmol, 1 equiv.) and TIPF$_6$ (16.36 mg, 0.046 mmol, 0.5 equiv.) in dichloromethane (10 mL) was stirred at room temperature for 1 h under the exclusion of light. Then, the solvent was removed under vacuum. The desired solid was isolated as a yellow crystalline solid. Yield: 89.4 mg (77 %). IR (ATR): ν(C≡C): 2099 cm^{-1}. HRMS ESI-TOF-MS (positive mode): 2361.7 [M]$^+$. Anal. Calcd. for C$_{96}$H$_{104}$N$_8$Au$_4$TlPF$_6$·3CH$_2$Cl$_2$ (2758.5): C, 43.07; H, 4.02; N, 4.06. Found: C, 43.09; H, 3.96; N, 4.03. ^{1}H NMR (400 MHz, 298 K, CDCl$_3$): δ 7.63 (d,

$^3J_{H-H}$ = 4.0 Hz, 2H, C*H*$_{anth}$), 7.43 (s, 1H, C*H*$_{anth}$), 7.35 (d, $^3J_{H-H}$ = 8.0 Hz, 2H, C*H*$_{anth,}$), 7.25 (s, 1H, C*H*$_{anth}$), 7.24 (dd, $^3J_{H-H}$ = 8.0 Hz, $^3J_{H-H}$ = 4.0 Hz, 2H, C*H*$_{anth}$), 6.66-6.59 (m, 4H, C*H*$_{Ph}$), 6.09-6.01 (m, 4H, C*H*$_{Ph}$), 4.63-4.33 (m, 8H, NC*H*$_2$CH$_2$CH$_2$CH$_3$), 1.72-1.60 (m, 8H, NCH$_2$C*H*$_2$CH$_2$CH$_3$), 1.39-1.26 (m, 8H, NCH$_2$CH$_2$C*H*$_2$CH$_3$), 0.94 (t, $^3J_{H-H}$ = 8.0 Hz, 12H, NCH$_2$CH$_2$CH$_2$C*H*$_3$). ^{19}F NMR (376 MHz, 298 K, CDCl$_3$): δ -73.84. ^{13}C NMR (100 MHz, 298 K, CDCl$_3$): δ 188.66 (Au-*C*$_{carbene}$), 133.51 (*C*$_{q\ anth}$), 131.88 (*C*H_{anth}), 130.67 (*C*$_{q\ Ph}$), 129.17 (*C*$_{q\ anth}$), 128.05 (*C*H_{anth}), 128.00 (*C*H_{anth}), 125.11 (*C*$_{q\ anth}$), 124.62 (*C*H_{anth}), 124.51 (*C*H_{anth}), 123.29 (*C*H_{Ph}), 112.03 (*C*$_{q\ acetylide}$), 111.64 (*C*$_{q\ acetylide}$), 109.69 (*C*H_{Ph}), 48.62 (N*C*H$_2$CH$_2$CH$_2$CH$_3$), 32.41 (NCH$_2$*C*H$_2$CH$_2$CH$_3$), 20.46 (NCH$_2$CH$_2$*C*H$_2$CH$_3$), 13.92 (NCH$_2$CH$_2$CH$_2$*C*H$_3$).

Synthesis of 5. A solution of **3** (100.00 mg, 0.093 mmol, 1 equiv.) and AgBF$_4$ (9.21 mg, 0.046 mmol, 0.5 equiv.) in dichloromethane (20 mL) was stirred at room temperature for 1 h under the exclusion of light. Then, the solvent was removed under vacuum. The desired solid was isolated as a yellow solid. Yield: 82.6 mg (76 %). IR (ATR): ν(C≡C): 2100 cm^{-1}. HRMS ESI-TOF-MS (positive mode): 2265.5 [M]$^+$. Anal. Calcd. for C$_{96}$H$_{104}$N$_8$Au$_4$AgBF$_4$·2CH$_2$Cl$_2$ (2518.5): C, 46.69; H, 4.32; N, 4.45. Found: C, 46.62; H, 4.26; N, 4.39. ^{1}H NMR (500 MHz, 253 K, CDCl$_3$): δ 9.33 (s, 1H, C*H*$_{anth}$), 7.66-7.58 (m, 2H, C*H*$_{anth}$), 7.19-7.13 (m, 4H, C*H*$_{anth}$ and C*H*$_{anth}$), 7.11 (s, 1H, C*H*$_{anth}$), 6.85-6.77 (m, 4H, C*H*$_{Ph}$), 6.24-6.15 (m, 4H, C*H*$_{Ph}$), 4.95 (br s, 4H, NC*H*$_2$CH$_2$CH$_2$CH$_3$), 3.08 (br s, 4H, NC*H*$_2$CH$_2$CH$_2$CH$_3$), 1.54-1.41 (m, 8H, NCH$_2$C*H*$_2$CH$_2$CH$_3$), 1.33-1.18 (m, 8H, NCH$_2$CH$_2$C*H*$_2$CH$_3$), 0.87 (t, $^3J_{H-H}$ = 8.0 Hz, 12H, NCH$_2$CH$_2$CH$_2$C*H*$_3$). ^{19}F NMR (282 MHz, 298 K, CDCl$_3$): δ -154.66. ^{13}C NMR (126 MHz, 253 K, CDCl$_3$): δ 191.15 (Au-*C*$_{carbene}$), 131.32 (*C*H_{anth}), 129.56 (*C*$_{q\ Ph}$), 129.04 (*C*$_{q\ anth}$), 128.89 (*C*$_{q\ anth}$), 128.10 (*C*H_{anth}), 127.40 (*C*H_{anth}), 127.25 (*C*H_{anth}), 125.35 (*C*H_{anth}), 124.70 (*C*$_{q\ acetylide}$), 123.58 (*C*$_{q\ anth}$), 123.01 (*C*H_{Ph}), 114.20 (*C*$_{q\ acetylide}$), 109.99 (*C*H_{Ph}), 47.62 (N*C*H$_2$CH$_2$CH$_2$CH$_3$), 31.92 (NCH$_2$*C*H$_2$CH$_2$CH$_3$), 20.31 (NCH$_2$CH$_2$*C*H$_2$CH$_3$), 13.89 (NCH$_2$CH$_2$CH$_2$*C*H$_3$).

Synthesis of 6. A solution of **3** (100.00 mg, 0.093 mmol, 1 equiv.) and [Cu(MeCN)$_4$]BF$_4$ (14.58 mg, 0.046 mmol, 0.5 equiv.) in dichloromethane (10 mL) was stirred at room temperature for 1 h under the exclusion of light. Then, the solvent was removed under vacuum. The desired solid was isolated as an orange solid. Yield: 91.1 mg (85 %). IR (ATR): ν(C≡C): 2103 cm^{-1}. HRMS ESI-TOF-MS (positive mode): 2220.6 [M]$^+$. Anal. Calcd. for C$_{96}$H$_{104}$N$_8$Au$_4$CuBF$_4$·2CH$_2$Cl$_2$ (2558.5): C, 46.43; H, 4.33; N, 4.38. Found: C, 46.43; H, 4.38; N, 4.36. ^{1}H NMR (500 MHz, 253 K, CDCl$_3$): δ 10.18 (s, 1H, C*H*$_{anth}$), 8.05 (d, $^3J_{H-H}$ = 5.0 Hz, 2H, C*H*$_{anth}$), 7.54-7.43 (m, C*H*$_{anth,}$ (c)), 7.37-7.27 (m, 4H, C*H*$_{Ph}$), 7.25-7.18 (m, 2H, C*H*$_{anth}$), 6.99-6.86 (m, 4H, C*H*$_{Ph}$), 6.76 (s, 1H, C*H*$_{anth}$), 3.35-3.14 (m, 4H, NC*H*$_2$CH$_2$CH$_2$CH$_3$), 3.14-2.97 (m, 4H, NC*H*$_2$CH$_2$CH$_2$CH$_3$), 1.52-1.29 (m, 8H, NCH$_2$C*H*$_2$CH$_2$CH$_3$), 1.10-0.90 (m, 8H, NCH$_2$CH$_2$C*H*$_2$CH$_3$), 0.84-0.70 (m, 12H, NCH$_2$CH$_2$CH$_2$C*H*$_3$). ^{19}F NMR (282 MHz, 298 K, CDCl$_3$): δ -153.45. ^{13}C NMR (126 MHz, 253 K, CDCl$_3$): δ 187.43 (Au-*C*$_{carbene}$), 134.53 (*C*H_{anth}), 132.28 (*C*$_{q\ anth}$), 130.41 (*C*H_{anth}), 130.63 (*C*$_{q\ ph}$), 129.94 (*C*H_{anth}), 128.72 (*C*$_{q\ anth}$), 126.00 (*C*H_{anth}), 125.13 (*C*H_{anth}), 124.51 (*C*H_{Ph}), 113.50 (*C*$_{q\ acetylide}$), 113.40 (*C*$_{q\ acetylide}$), 111.26 (*C*H_{Ph}), 46.89 (N*C*H$_2$CH$_2$CH$_2$CH$_3$), 31.49 (NCH$_2$*C*H$_2$CH$_2$CH$_3$), 20.04 (NCH$_2$CH$_2$*C*H$_2$CH$_3$), 13.80 (NCH$_2$CH$_2$CH$_2$*C*H$_3$).

Synthesis of 7. A solution of **3** (100.00 mg, 0.093 mmol, 1 equiv.) and AgBF$_4$ (18.42 mg, 0.093 mmol, 1 equiv.) in dichloromethane (20 mL) was stirred at room temperature for 1 h under the exclusion of light. The suspension was filtered through a pad of Celite and the solvent removed under vacuum. The desired solid was isolated as an orange solid. Yield: 80.9 mg (68 %). Complex **7** is soluble in chlorinated solvents but suffered decomposition within hours. IR (ATR): ν(C≡C): 2099 cm^{-1}. HRMS ESI-TOF-MS (positive mode): 1186.3 [M$_2$]$^{2+}$ and 2265.5 [M]$^+$. Anal. Calcd. for C$_{48}$H$_{52}$N$_4$Au$_2$AgBF$_4$ 2CH$_2$Cl$_2$ (1440.2): C, 41.66; H, 3.92; N, 3.88. Found: C, 41.59; H, 3.92; N, 3.99. ^{1}H NMR (500 MHz, 253 K, CDCl$_3$): δ 9.70 (s,

1H, C*H*~anth~), 7.97-7.86 (m, 2H, C*H*~anth~), 7.64-7.46 (m, 4H, C*H*~anth~ and C*H*~anth~), 6.84-6.69 (m, 4H, C*H*~Ph~), 4.62-4.51 (m, 4H, NC*H*$_2$CH$_2$CH$_2$CH$_3$), 3.49 (br s, 4H, NC*H*$_2$CH$_2$CH$_2$CH$_3$), 2.03-1.77 (m, 8H, NCH$_2$C*H*$_2$CH$_2$CH$_3$), 1.57-1.33 (m, 8H, NCH$_2$CH$_2$C*H*$_2$CH$_3$), 1.10-0.92 (m, 12H, NCH$_2$CH$_2$CH$_2$C*H*$_3$). ^{19}F NMR (282 MHz, 298 K, CDCl$_3$): δ -153.49. ^{13}C NMR (126 MHz, 253 K, CDCl$_3$): δ 187.29 (Au-*C*~carbene~), 131.22 (*C*H~anth~), 129.61 (*C*~q Ph~), 129.41 (*C*~q anth~), 128.48 (*C*H~anth~),126.33 (*C*~q anth~),125.56 (*C*H~anth~), 125.22 (*C*H~anth~), 125.13 (*C*H~anth~), 124.35 (*C*H~Ph~), 116.12 (*C*~q acetylide~), 111.95 (*C*~q anth~), 111.33 (*C*H~Ph~), 109.98 (*C*~q acetylide~), 47.38 (N*C*H$_2$CH$_2$CH$_2$CH$_3$), 31.45 (NCH$_2$*C*H$_2$CH$_2$CH$_3$), 20.24 (NCH$_2$CH$_2$*C*H$_2$CH$_3$), 13.88 (NCH$_2$CH$_2$CH$_2$*C*H$_3$).

Titration experiments

^{1}H NMR titration experiments. The experiments were carried out in CDCl$_3$, at constant concentrations of the host (1 mM). Two solutions were prepared: solution A (only containing **3** at 1 mM) and solution B (containing host at 1 mM and guest at 10 mM). The addition of increasing amounts of solution B to solution A produced a perturbation of some of the proton resonances of the host.

UV-visible titrations. The experiments were carried out in degassed CH$_2$Cl$_2$, at constant concentrations of the host (1x10^{-5}). Two solutions were prepared: solution A (only containing **3**) and solution B (containing host at 1x10^{-5} M, and guest at 1x10^{-4} M). The addition of increasing amounts of solution B to solution A produced a perturbation of the absorption spectra of the host. The association constants were obtained by nonlinear least-square analysis by using the HypSpec2014 program. Three different Host:Guest models were used for each titration (1:1, 1:2 and 2:1), and in all cases the model was chosen according to the best fitting and by comparing the distribution of residual errors.

Fluorescence titrations. The experiments were carried out in degassed CH$_2$Cl$_2$, at constant concentrations of the host (1x10^{-5} M). Two solutions were prepared: solution A (only containing **3**) and solution B (containing host at 1x10^{-5} M, and guest at 1x10^{-4} M). The addition of increasing amounts of solution B to solution A produced a perturbation of the emission spectra of the host. The association constants were obtained by nonlinear least-square analysis by using the HypSpec2014 program. Three different Host:Guest models were used for each titration (1:1, 1:2 and 2:1), and in all cases the model was chosen according to the best fitting and by comparing the distribution of residual errors.

[1] a) D. L. Caulder and K. N. Raymond, *Acc. Chem. Res.* **1999**, *32*, 975-982; b) L. Chen, Q. Chen, M. Wu, F. Jiang and M. Hong, *Acc. Chem. Res.* **2015**, *48*, 201-210; c) M. Mauro, A. Aliprandi, D. Septiadi, N. S. Kehra and L. De Cola, *Chem. Soc. Rev.* **2014**, *43*, 4144-4166; d) M. L. Saha, S. De, S. Pramanik and M. Schmittel, *Chem. Soc. Rev.* **2013**, *42*, 6860-6909; e) R. Chakrabarty, P. S. Mukherjee and P. J. Stang, *Chem. Rev.* **2011**, *111*, 6810-6918; f) S. Leininger, B. Olenyuk and P. J. Stang, *Chem. Rev.* **2000**, *100*, 853-907; g) P. J. Stang and B. Olenyuk, *Acc. Chem. Res.* **1997**, *30*, 502-518; h) B. Linton and A. D. Hamilton, *Chem. Rev.* **1997**, *97*, 1669-1680; i) M. R. Johnston and M. J. Latter, *Supramol. Chem.* **2005**, *17*, 595-607; j) D. W. Johnson and K. N. Raymond, *Supramol. Chem.* **2001**, *13*, 639-659.

[2] a) A. Aliprandi, M. Mauro and L. De Cola, *Nat. Chem.* **2016**, *8*, 10-15; b) K. Jie, Y. Zhou, Y. Yao, B. Shi and F. Huang, *J. Am. Chem. Soc.* **2015**, *137*, 10472-10475; c) X. Yan, T. R. Cook, J. B. Pollock, P. Wei, Y. Zhang, Y. Yu, F. Huang and P. J. Stang, *J. Am. Chem. Soc.* **2014**, *136*, 4460-4463; d) X. Yan, S. Li, T. R. Cook, X. Ji, Y. Yao, J. B. Pollock, Y. Shi, G. Yu, J. Li, F. Huang and P. J. Stang, *J. Am. Chem. Soc.* **2013**, *135*, 14036-14039.

[3] a) G. Kumar and R. Gupta, *Chem. Soc. Rev.* **2013**, *42*, 9403-9453; b) M. C. Das, S. C. Xiang, Z. J. Zhang and B. L. Chen, *Angew. Chem. Int. Ed.* **2011**, *50*, 10510-10520; c) S. Srivastava and R. Gupta, *Crystengcomm* **2016**, *18*, 9185-9208.

[4] a) H. Schmidbaur and A. Schier, *Chem. Soc. Rev.* **2012**, *41*, 370-412; b) H. Schmidbaur and A. Schier, *Chem. Soc. Rev.* **2008**, *37*, 1931-1951; c) H. Schmidbaur and A. Schier, *Angew. Chem. Int. Ed.* **2015**, *54*, 746-784; d) S. Sculfort and P. Braunstein, *Chem. Soc. Rev.* **2011**, *40*, 2741-2760; e) C. Silvestru and A. Laguna in *The Chemistry of Gold-Gold Metal Bonds*, *Vol.* John Wiley & Sons, **2015**.

[5] a) M. J. Katz, K. Sakai and D. B. Leznoff, *Chem. Soc. Rev.* **2008**, *37*, 1884-1895; b) E. R. T. Tiekink, *Coord. Chem. Rev.* **2014**, *275*, 130-153.

[6] a) R. Donamaria, E. J. Fernandez, J. M. Lopez-de-Luzuriaga, M. Monge, M. E. Olmos, D. Pascual and M. Rodriguez-Castillo, *Dalton Trans.* **2017**, *46*, 10941-10949; b) R. Galassi, M. M. Ghimire, B. M. Otten, S. Ricci, R. N. McDougald, R. M. Almotawa, D. Alhmoud, J. F. Ivy, A. M. M. Rawashdeh, V. N. Nesterov, E. W. Reinheimer, L. M. Daniels, A. Burini and M. A. Omary, *Proc. Natl. Acad. Sci. U. S. A.* **2017**, *114*, E5042-E5051; c) M. Gil-Moles, M. C. Gimeno, J. M. Lopez-de-Luzuriaga, M. Monge, M. E. Olmos and D. Pascual, *Inorg. Chem.* **2017**, *56*, 9281-9290; d) I. O. Koshevoy, Y. C. Chang, A. J. Karttunen, M. Haukka, T. Pakkanen and P. T. Chou, *J. Am. Chem. Soc.* **2012**, *134*, 6564-6567; e) A. Laguna, T. Lasanta, J. M. Lopez-de-Luzuriaga, M. Monge, P. Naumov and M. E. Olmos, *J. Am. Chem. Soc.* **2010**, *132*, 456-+; f) T. Lasanta, M. E. Olmos, A. Laguna, J. M. Lopez-de-Luzuriaga and P. Naumov, *J. Am. Chem. Soc.* **2011**, *133*, 16358-16361; g) S. Y. L. Leung and V. W. W. Yam, *Chem. Sci.* **2013**, *4*, 4228-4234; h) R. J. Roberts, D. Le and D. B. Leznoff, *Chem. Commun.* **2015**, *51*, 14299-14302; i) Y. Tanaka, K. M. C. Wong and V. W. W. Yam, *Chem. Sci.* **2012**, *3*, 1185-1191; j) X. F. Jiang, F. K. W. Hau, Q. F. Sun, S. Y. Yu and V. W. W. Yam, *J. Am. Chem. Soc.* **2014**, *136*, 10921-10929; k) O. S. Wenger, *Chem. Rev.* **2013**, *113*, 3686-3733; l) X. Zhang, B. Li, Z.-H. Chen and Z.-N. Chen, *J. Mater. Chem.* **2012**, *22*, 11427-11441; m) X. M. He and V. W. W. Yam, *Coord. Chem. Rev.* **2011**, *255*, 2111-2123; n) V. W. W. Yam, V. K. M. Au and S. Y. L. Leung, *Chem. Rev.* **2015**, *115*, 7589-7728.

[7] J. C. Lima and L. Rodriguez, *Chem. Soc. Rev.* **2011**, *40*, 5442-5456.

[8] J. Gil-Rubio and J. Vicente, *Chem. Eur. J.* **2018**, *24*, 32-46.

[9] S. Ibañez, M. Poyatos and E. Peris, *Angew. Chem. Int. Ed.* **2017**, *56*, 9786-9790.

[10] C. Biz, S. Ibañez, M. Poyatos, D. Gusev and E. Peris, *Chem. Eur. J.* **2017**, *23*, 14439-14444.

[11] a) A. K.-W. Chan, W. H. Lam, Y. Tanaka, K. M.-C. Wong and V. W.-W. Yam, *Proc. Natl. Acad. Sci. U. S. A.* **2015**, *112*, 690-695; b) F. K. W. Kong, A. K. W. Chan, M. Ng, K. H. Low and V. W. W. Yam, *Angew. Chem. Int. Ed.* **2017**, *56*, 15103-15107; c) Z. J. Li, Y. F. Han, Z. C. Gao and F. Wang, *ACS Catal.* **2017**, *7*, 4676-4681; d) X. Zhang, L. Ao, Y. F. Han, Z. Gao and F. Wang, *Chem. Commun.* **2018**, 1754-1757.

[12] a) H. de la Riva, M. Nieuwhuyzen, C. M. Fierro, P. R. Raithby, L. Male and M. C. Lagunas, *Inorg. Chem.* **2006**, *45*, 1418-1420; b) G. F. Manbeck, W. W. Brennessel, R. A. Stockland and R. Eisenberg, *J. Am. Chem. Soc.* **2010**, *132*, 12307-12318.

[13] V. Mishra, A. Raghuvanshi, A. K. Saini and S. M. Mobin, *J. Organomet. Chem.* **2016**, *813*, 103-109.

[14] a) A. J. Lowe, F. M. Pfeffer and P. Thordarson, *Supramol. Chem.* **2012**, *24*, 585-594; b) P. Thordarson, *Chem. Soc. Rev.* **2011**, *40*, 1305-1323.

[15] a) K. Chen, C. E. Strasser, J. C. Schmitt, J. Shearer and V. J. Catalano, *Inorg. Chem.* **2012**, *51*, 1207-1209; b) C. E. Strasser and V. J. Catalano, *J. Am. Chem. Soc.* **2010**, *132*, 10009-10011; c) R. R. Ramazanov, A. I. Kononov, A. M. Nesterenko, J. R. Shakirova, I. O. Koshevoy, E. V. Grachova and S. P. Tunik, *J. Phys. Chem. C* **2016**, *120*, 25541-25547; d) J. R. Shakirova, E. V. Grachova, A. S. Melnikov, V. V. Gurzhiy, S. P. Tunik, M. Haukka, T. A. Pakkanen and I. O. Koshevoy, *Organometallics* **2013**, *32*, 4061-4069.

[16] I. O. Koshevoy, Y.-C. Chang, A. J. Karttunen, J. R. Shakirova, J. Janis, M. Haukka, T. Pakkanen and P.-T. Chou, *Chem. Eur. J.* **2013**, *19*, 5104-5112.

[17] J. H. Lamm, J. Glatthor, J. H. Weddeling, A. Mix, J. Chmiel, B. Neumann, H. G. Stammler and N. W. Mitzel, *Org. Bio. Chem.* **2014**, *12*, 7355-7365.

[18] S. Ibañez, M. Poyatos and E. Peris, *Organometallics* **2017**, *36*, 1447-1451.

[19] G. J. Kubas, *Inorg. Synth.* **1990**, *28*, 68-70.

FULL PAPER

The complex supramolecular landscape of a di-gold metallo-tweezer is controlled by adding a series of metal cations. The choice of the cation is used to directing the formation of the designated molecular architecture.

An exceptional supramolecular tunable scaffold for:

➢ Self-aggregated dimers
➢ Oligomers
➢ Polymers
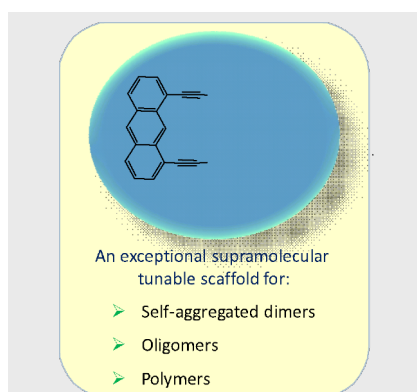
Susana Ibáñez and Eduardo Peris*

Page No. – Page No.

Chemically-tunable formation of different discrete, oligomeric and polymeric self-assembly structures from a di-gold metallo-tweezer